Supporting Information for

Layer-by-Layer Assembly of Exfoliated Layered Double Hydroxide Nanosheets for Enhanced Electrochemical Oxidation of Water

Cong Zhang,‡[a] Jingwen Zhao,‡[b] Lei Zhou,[a] Zhenhua Li,[a] Mingfei shao*[a] and Min Wei*[a]

a. State Key Laboratory of Chemical Resource Engineering, Beijing University of Chemical Technology, Beijing 100029, P. R. China. E-mail: shaomf@mail.buct.edu.cn (Mingfei Shao), weimin@mail.buct.edu.cn (Min Wei); Fax: +86-10-64425385; Tel: +86-10-64412131

b. Qingdao Industrial Energy Storage Research Institute, Qingdao Institute of Bioenergy and Bioprocess Technology, Chinese Academy of Science, Qingdao 266101, P. R. China.

* Corresponding authors. Tel: +86-10-64412131; Fax: +86-10-64425385.

E-mail addresses: shaomf@mail.buct.edu.cn (Mingfei Shao); weimin@mail.buct.edu.cn (Min Wei).

‡ Contributed equally to this work.

Experimental details

Fabrication of LDH NSs collide solution. The CoNi-LDH with Br^- anions was prepared via a topochemical approach.[1] CoMn, CoFe and ZnCo LDHs with CO_3^{2-} anions were synthesized via a coprecipitation method.[2-4] To prepare the NO_3^-

intercalated LDHs, the as-prepared 0.2 g CO_3^{2-} anions (Br^- for CoNi-LDH) intercalated LDHs powder was further added into a flask containing 0.3 mol of $NaNO_3$ into 200 mL of ethanol/water binary liquid (1:1, v/v). The flask was mechanically shaken at room temperature in nitrogen atmosphere for 48 h. The product was filtered, washed with anhydrous ethanol, and dried in the air. The exfoliation was performed as follows: a 0.05 g of LDH-NO_3 was dispersed in 100 mL of formamide in a flask sealed in nitrogen atmosphere, and then agitated in a mechanical shaker for 60 h, giving a colloidal suspension. The resulting translucent colloidal solution was further centrifugated to remove possible unexfoliated LDH particles.

For obtaining CoNi-LDH with different Co content, the amount of $CoCl_2 \cdot 6H_2O$ used in the synthesis was changed from 5.0 to 3.3 and 2.5 mM, respectively, and the corresponding amount of $NiCl_2 \cdot 6H_2O$ was also changed from 2.5 to 3.3 and 5.0 mM, respectively, to keep the molar ratio of Co^{2+} to Ni^{2+} to be 2:1, 1:1 and 1:2, respectively. The final products were denoted as Co_2Ni-LDH, CoNi-LDH, and $CoNi_2$-LDH. For obtaining CoNi-LDH with different Co^{3+} content, the amount of Br_2 used in oxidation of Co_2Ni hydroxide was changed from 3.5 to 10.5 mM, respectively.

The fabrication of CoNi-LDH/Fe-PP-M electrode. CoNi-LDH NSs colloidal solution and Fe-PP solution were mixed with equal molar ratio under constant stirring. After stirring for 12 h accompanied in nitrogen atmosphere, the dark brown precipitate was centrifuged at 9000 rpm, and washed by deionized Milli-Q water. Then disperse the precipitate in ethanol absolute with nafion, and drop a

complete coverage layer on ITO glass. The obtained CoNi-LDH/Fe-PP-M electrode was dried in air.

The fabrication of CoNi-LDH electrode. ITO glass was overspread with the CoNi-LDH NSs colloidal solution, and then dried at 125℃ for several days until all formamide volatilized. Finally, the CoNi-LDH electrode was obtained. The mass-loading of CoNi-LDH/Fe-PP-M and CoNi-LDH NSs catalyst was controlled by repeating the droping process for several cycles to obtain the same total mass of CoNi-LDH as in $(CoNi\text{-}LDH/Fe\text{-}PP)_{30}$ UTF (0.12 mg cm^{-2}).

The fabrication of CoNi-LDH/CO_3^{2-}, CoNi-LDH/NO_3^-, CoNi-LDH/PSS and CoNi-LDH/SDS electrodes. The assembly process for CoNi-LDH/CO_3^{2-}, CoNi-LDH/NO_3^-**,** CoNi-LDH/PSS and CoNi-LDH/SDS UTFs modified ITO electrodes is similar to $(CoNi\text{-}LDH/Fe\text{-}PP)_n$ UTFs modified electrode. In brief, the ITO glass substrate was dipped into a colloidal suspension of CoNi-LDH NSs (0.5 g L^{-1}) for 10 min followed by immersion into an aqueous solution of 0.5 M Na_2CO_3 ($NaNO_3$, poly(sodium styrene-4-sulfonate) (PSS) or sodium dodecyl sulfonate (SDS)) for another 10 min. Subsequently, the deposition operation was repeated *n* times to obtain a multilayer film of CoNi-LDH/CO_3^{2-}, CoNi-LDH/NO_3^-**,** CoNi-LDH/PSS and CoNi-LDH/SDS UTFs.

The fabrication of IrO_2 electrode. IrO_2 powders (5 mg) were dispersed in mixed solvent of deionized water (1 mL) and 2-propanol (0.25 mL) via sonication for more than 1 h. To increase the binding strength, 10 μL Nafion solution (5 wt%) was added into the IrO_2 powders suspension. Suspensions (35.4 μL) were then drop-casted on

ITO (1 cm^2), and the solvent was allowed to be evaporated at 40 ºC. The catalyst loading was 0.142 mg cm^{-2} on ITO glass electrode.

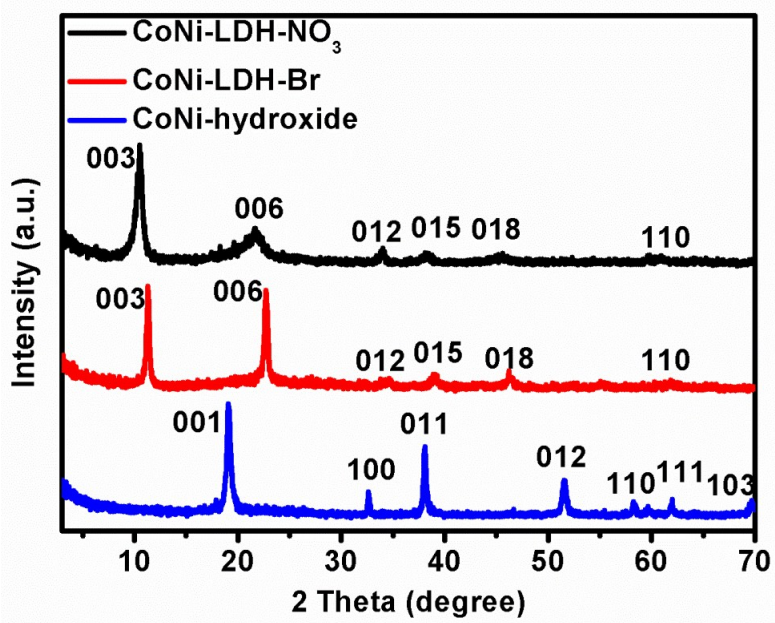

Fig. S1 X-ray powder diffraction patterns of CoNi-hydroxides, CoNi-LDH-Br, and CoNi-LDH-NO_3.

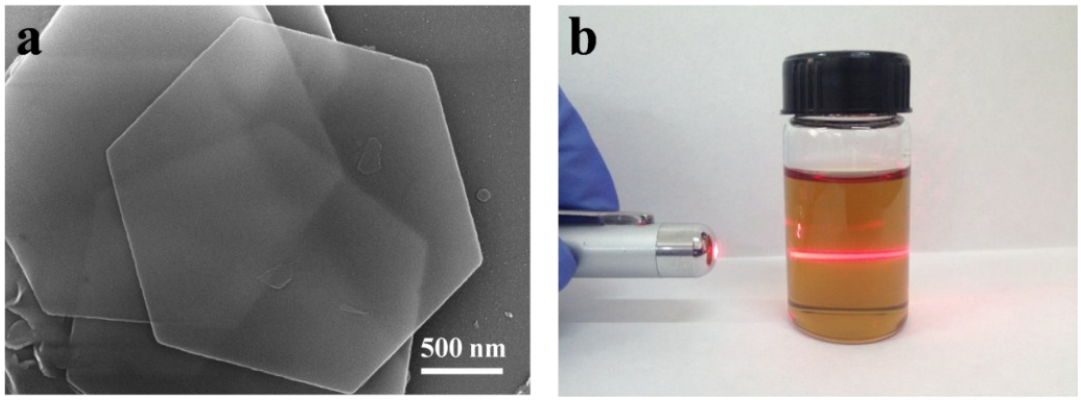

Fig. S2 (a) SEM image of CoNi-hydroxides. (b) Optical image of colloidal solutions of exfoliated CoNi-LDH NSs; Tyndall effect was observed when irradiated with a laser beam.

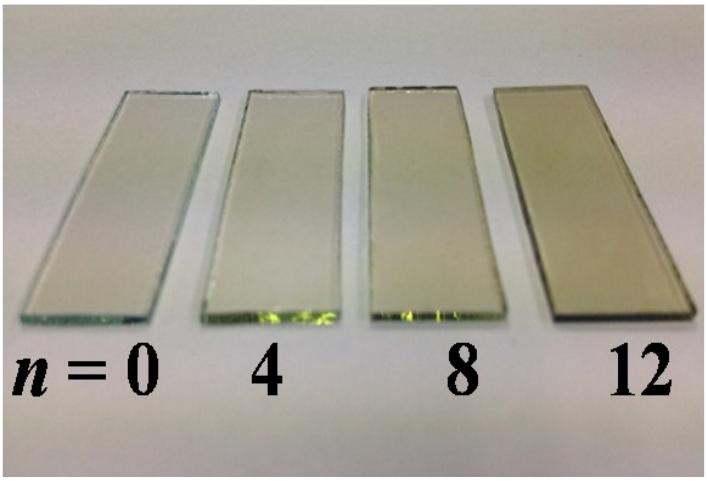

Fig. S3 The digital photograph of the $(CoNi\text{-}LDH/Fe\text{-}PP)_n$ UTFs ($n = 0 \sim 12$).

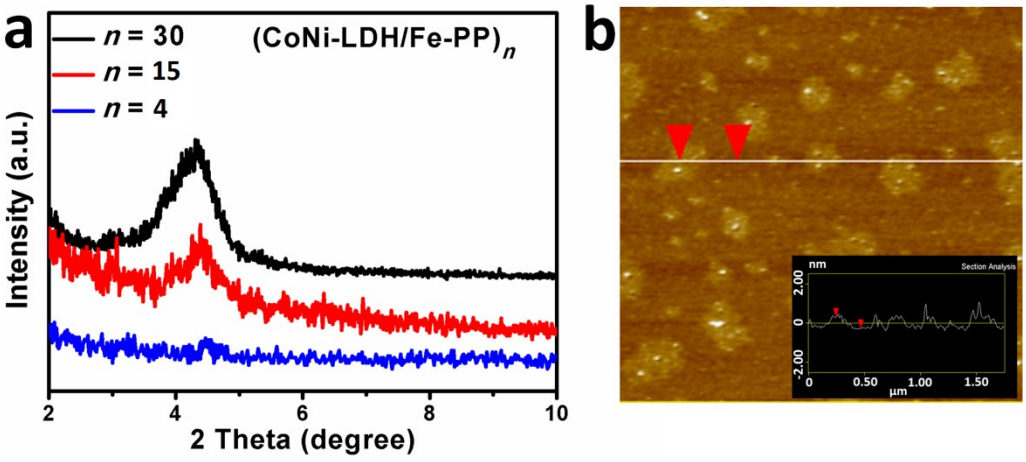

Fig. S4 (a) XRD patterns for the $(CoNi\text{-}LDH/Fe\text{-}PP)_n$ UTFs deposited on quartz glass substrates; (b) AFM image for exfoliated CoNi-LDH NSs.

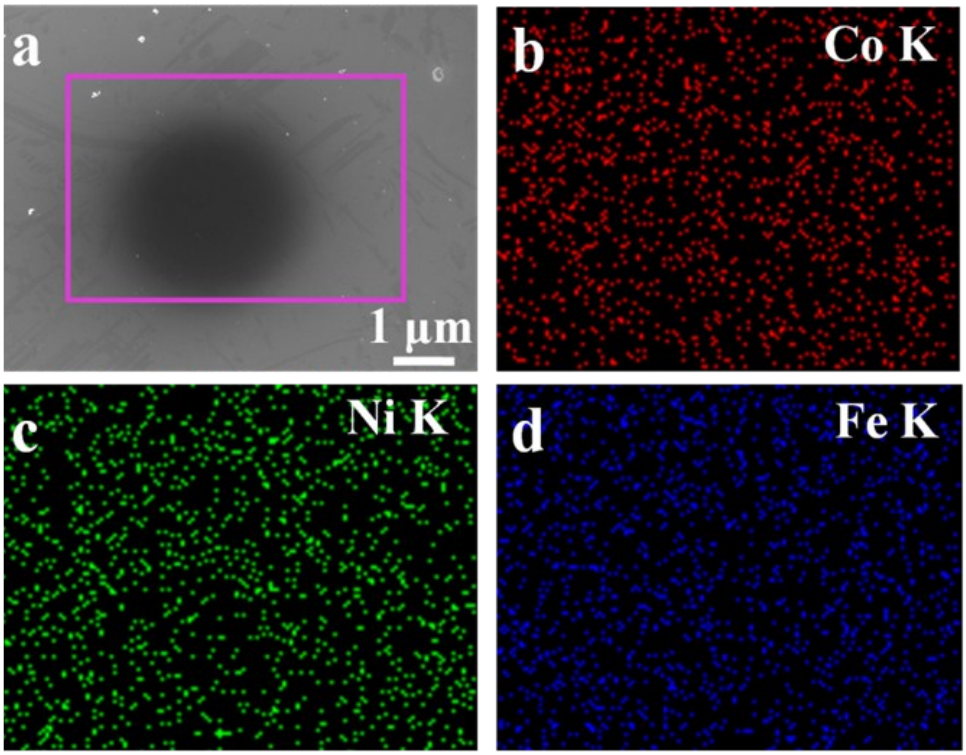

Fig. S5 SEM image of the $(CoNi\text{-}LDH/Fe\text{-}PP)_{10}$ UTF and corresponding EDS results.

Table S1 The elemental contents of EDS spectrum for $(CoNi\text{-}LDH/Fe\text{-}PP)_{10}$ UTF.

Element	Weight percent (%)	Atom percent (%)
O K	46.41	68.89
Fe K	8.33	3.23
Co K	28.86	12.64
Ni K	16.40	6.05

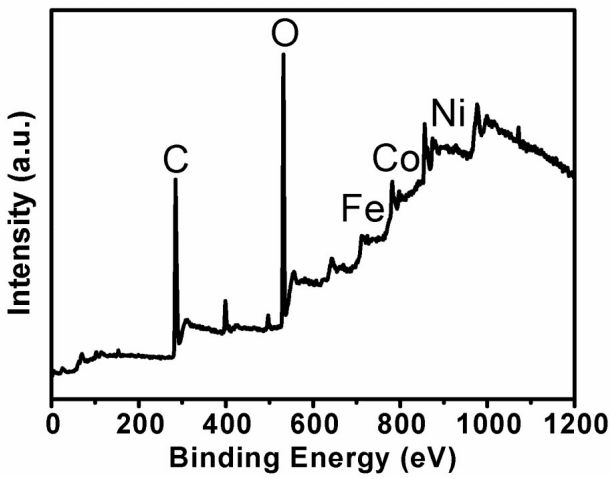

Fig. S6 XPS spectra of $(CoNi\text{-}LDH/Fe\text{-}PP)_{30}$ UTF.

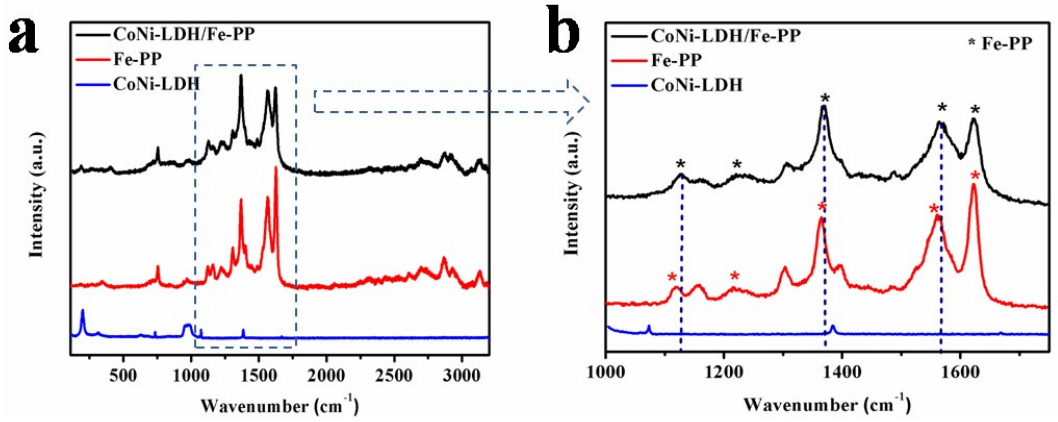

Fig. S7 (a) Raman spectra for the $(CoNi\text{-}LDH/Fe\text{-}PP)_n$ UTFs, pristine Fe-PP and CoNi-LDH NSs; (b) corresponding local enlargement of the Raman spectra at 1000-1750 cm^{-1}.

Table S2 Vibrational modes in the Raman spectrum of the $(CoNi\text{-}LDH/Fe\text{-}PP)_n$ UTFs.

Raman shift (cm^{-1})	Assignment
1120	$\delta(C_\alpha - H)$
1217	$\delta(C_m - ph)$
1363	$\Gamma(C_\alpha - N) + \delta(C_\beta - H)$
1560	$\Gamma(C_\beta - C_\beta) + \delta(C_\beta - H)$
1618	phenyl

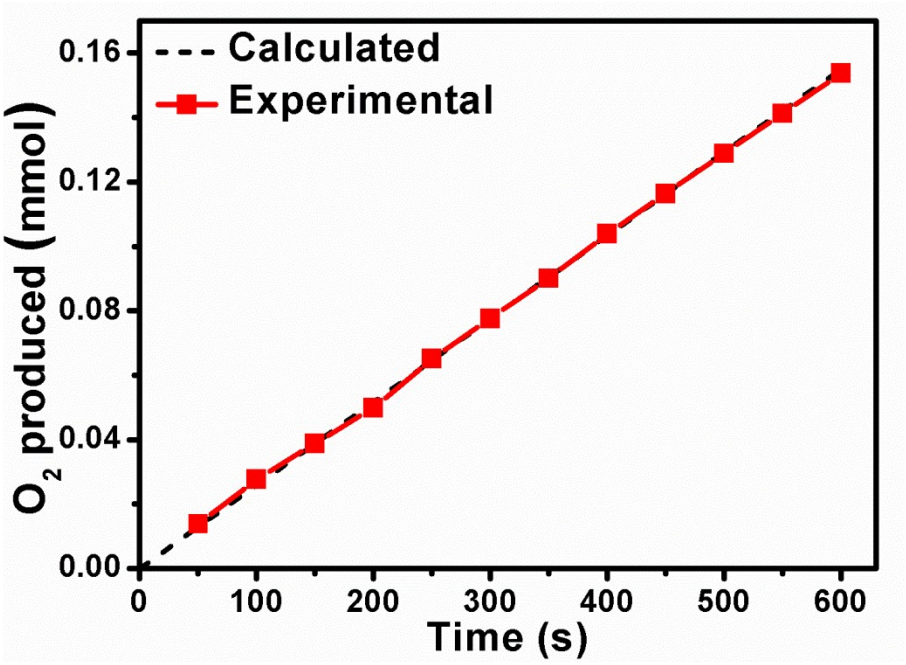

Fig. S8 Calculated and actual oxygen production catalyzed by $(CoNi\text{-}LDH/Fe\text{-}PP)_{30}$ UTF at a constant current of 100 mA cm^{-2}.

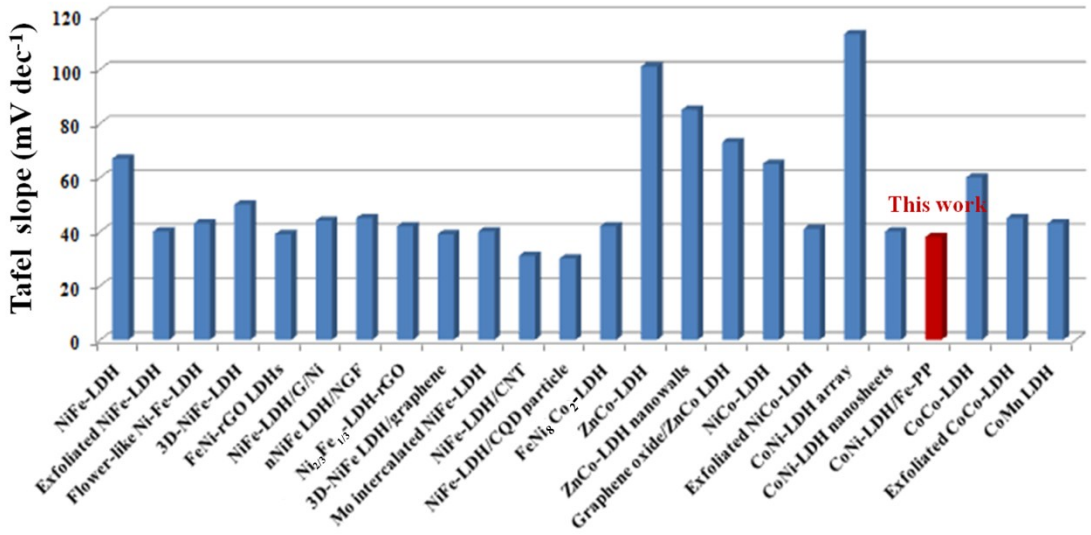

Fig. S9 Comparison of Tafel slopes in this work to the reported LDHs-based OER catalysts in alkali solution.[5-23]

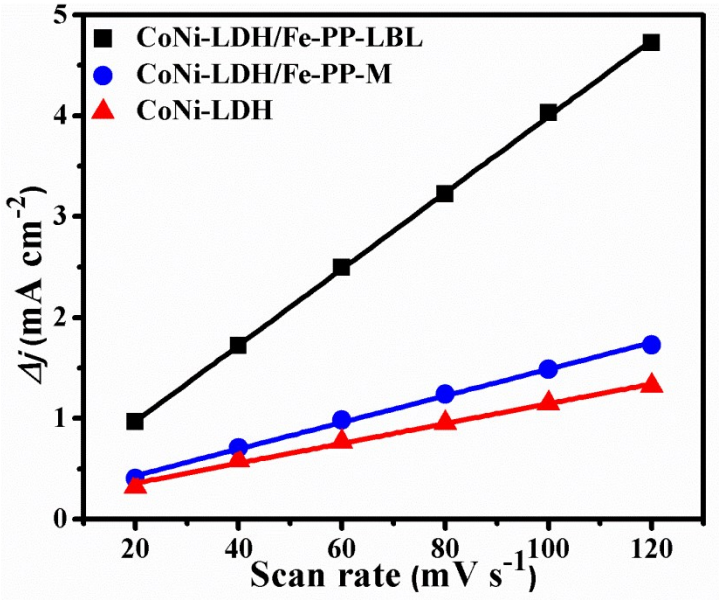

Fig. S10 Charging current density differences ($\Delta j = j_a - j_c$) plotted against scan rates. The linear slope is equivalent to twice of the double-layer capacitance C_{dl}.

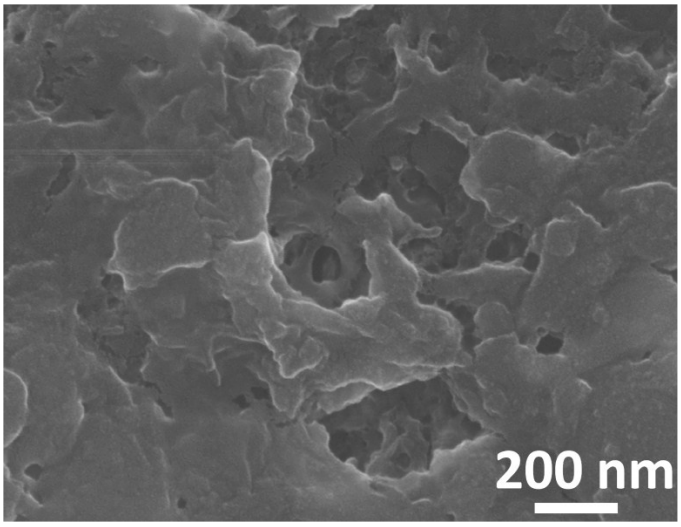

Fig. S11 SEM image of the CoNi-LDH drop on ITO substrate.

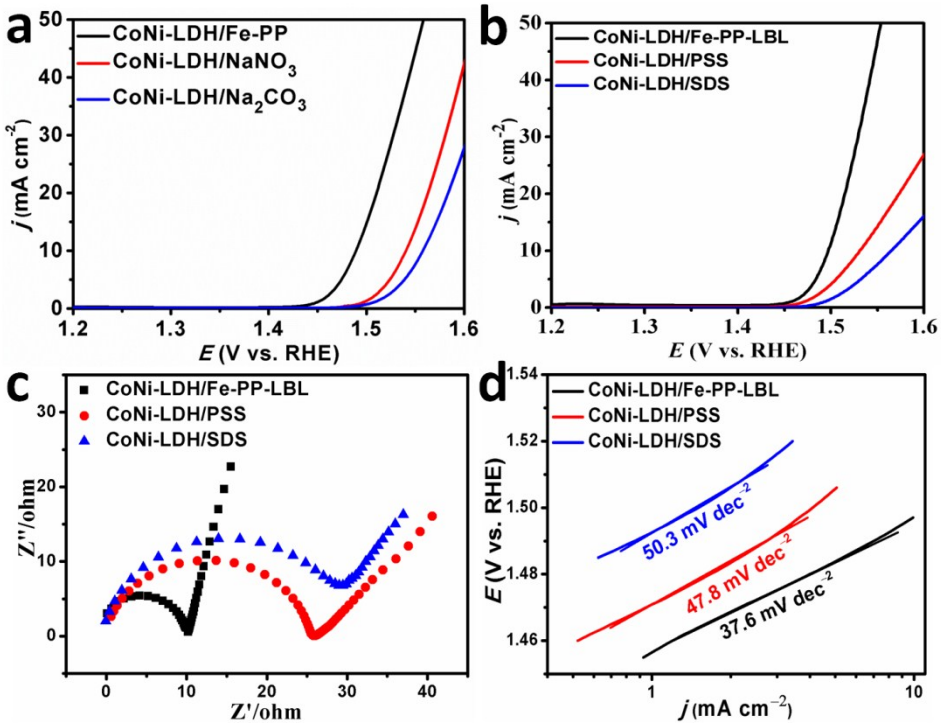

Fig. S12 (a) LSV curves of $(CoNi\text{-}LDH/Fe\text{-}PP)_{30}$ UTF, $(CoNi\text{-}LDH/NaNO_3)_{30}$ UTF and $(CoNi\text{-}LDH/Na_2CO_3)_{30}$ UTF; (b) LSV curves, (c) EIS curves and (d) Tafel slopes of $(CoNi\text{-}LDH/Fe\text{-}PP)_{30}$ UTF, $(CoNi\text{-}LDH/PSS)_{30}$ UTF and $(CoNi\text{-}LDH/Fe\text{-}SDS)_{30}$ UTF.

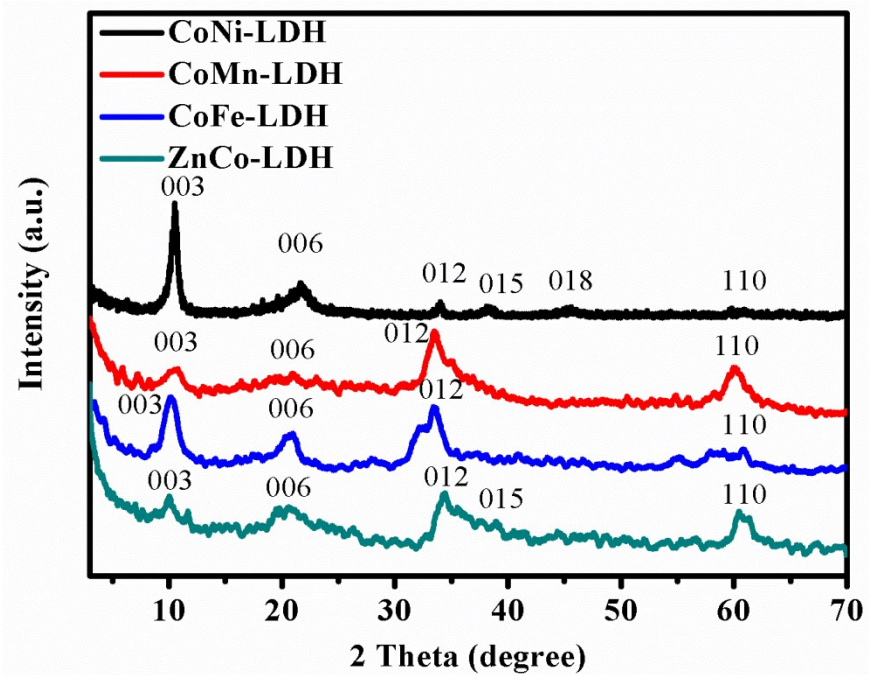

Fig. S13 XRD patterns of $CoNi\text{-}LDH\text{-}NO_3$, $CoMn\text{-}LDH\text{-}NO_3$, $CoFe\text{-}LDH\text{-}NO_3$ and $ZnCo\text{-}LDH\text{-}NO_3$ samples. The XRD patterns can be indexed to similar rhombohedral LDH phases. No other crystalline phase was detected, indicating the high purity of the CoNi-, CoMn-, CoFe- and ZnCo-LDH.

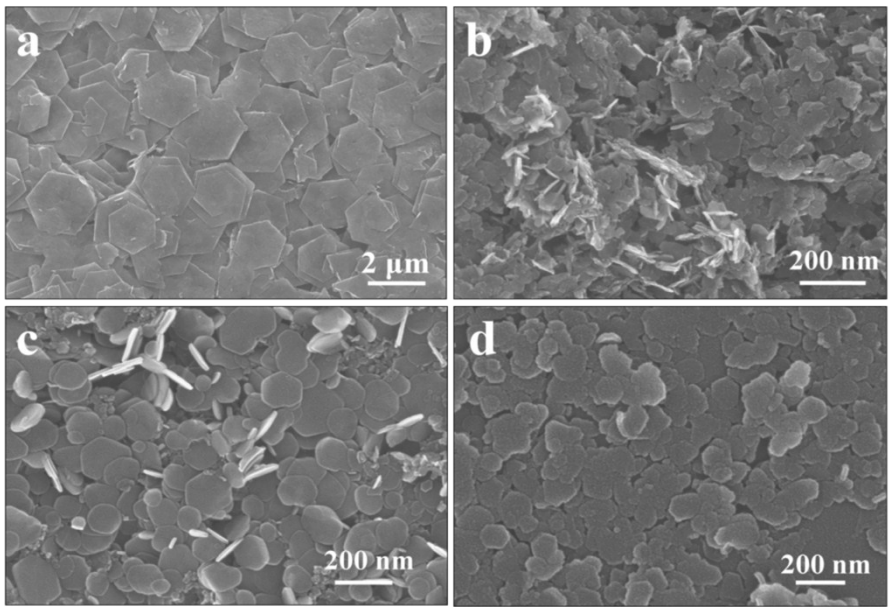

Fig. S14 SEM images for (a) CoNi-LDH-NO_3, (b) CoMn-LDH-NO_3, (c) CoFe-LDH-NO_3 and (d) ZnCo-LDH-NO_3. The typical SEM images of CoNi-, CoMn-, CoFe- and ZnCo-LDH reveal that the samples display hexagonal plate-like morphology with uniform lateral dimensions.

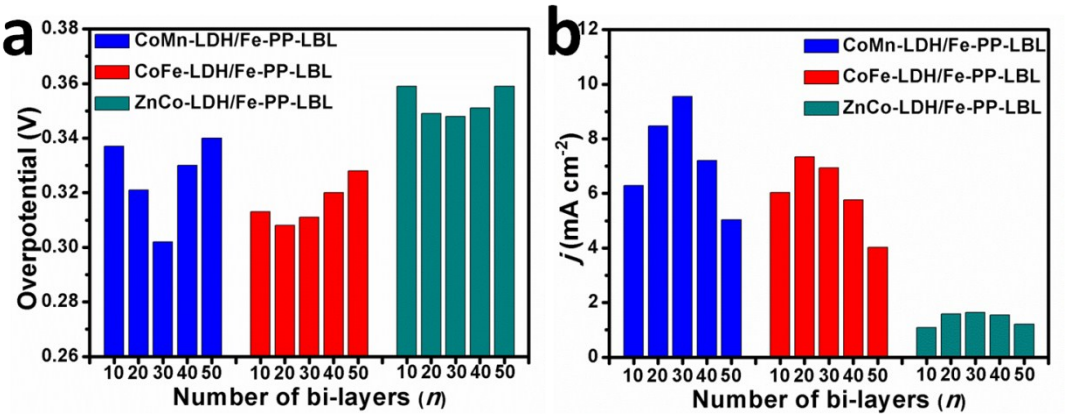

Fig. S15 (a) Current densities for the (CoMn-LDH/Fe-PP)$_n$, (CoFe-LDH/Fe-PP)$_n$ and (ZnCo-LDH/Fe-PP)$_n$ UTFs at η= 300 mV, n= 10, 20, 30, 40 and 50, respectively; (b) Overpotentials for the (CoMn-LDH/Fe-PP)$_n$, (CoFe-LDH/Fe-PP)$_n$ and (ZnCo-LDH/Fe-PP)$_n$ UTFs at j= 10 mA cm^{-1}, n= 10, 20, 30, 40 and 50, respectively.

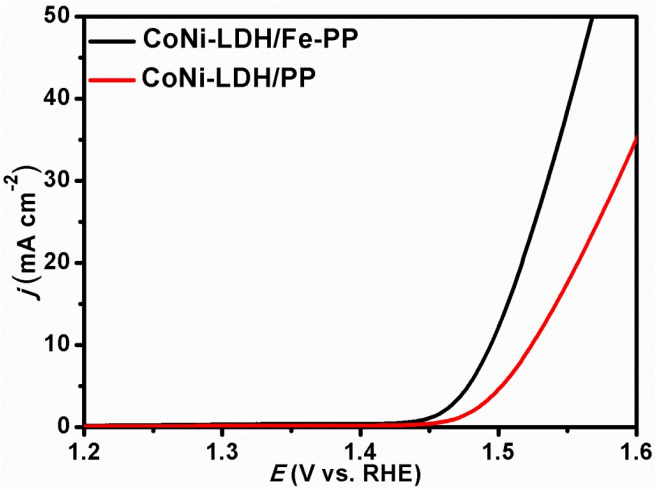

Fig. S16 LSV curves of $(CoNi\text{-}LDH/Fe\text{-}PP)_{30}$ UTF and $(CoNi\text{-}LDH/PP)_{30}$ UTF.

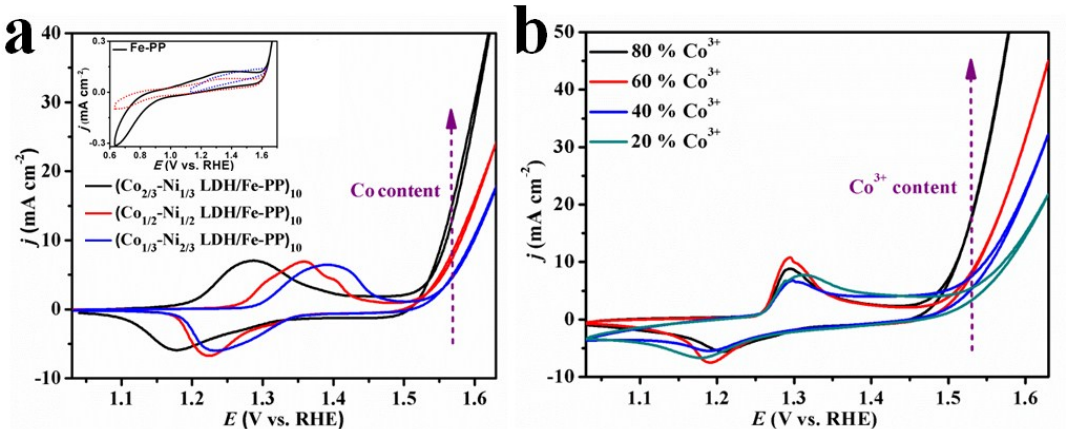

Fig. S17 Cyclic voltammograms of (a) CoNi-LDH/Fe-PP UTFs with different Co/Ni molar ratio (inset: cyclic voltammograms of Fe-PP in different sweep ranges); (b) CoNi-LDH/Fe-PP UTFs with different Co^{3+} content recorded at a potential sweep rate of 50 mV s^{-1}.

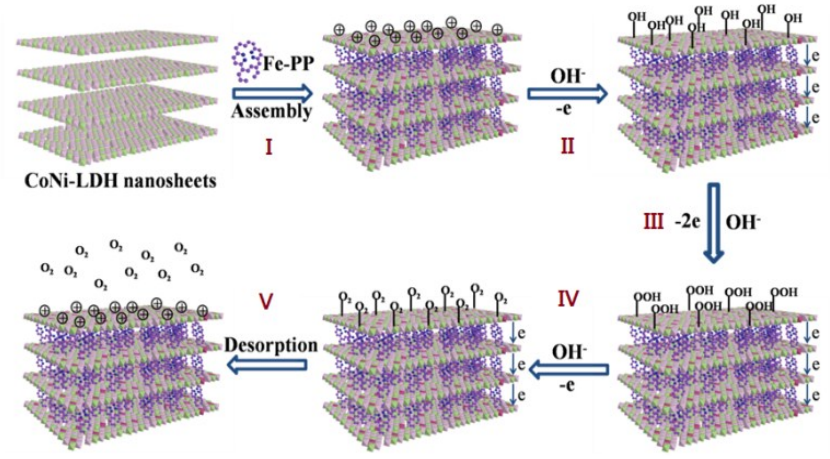

Scheme S1 Schematic illustration for OER electrocatalytic process of $(CoNi\text{-}LDH/Fe\text{-}PP)_n$ UTFs.

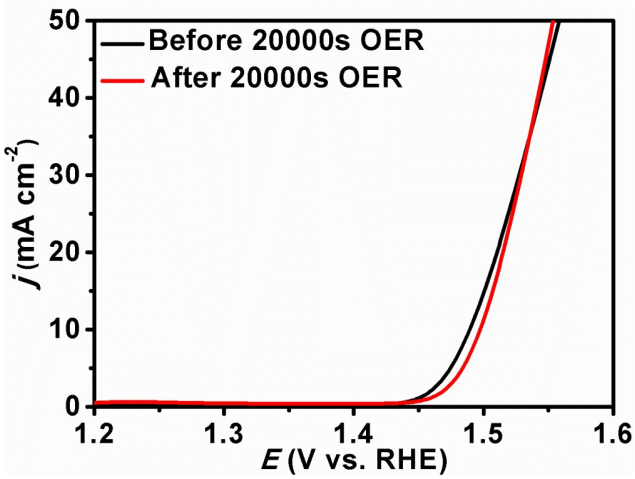

Fig. S18 LSV curves of $(CoNi\text{-}LDH/Fe\text{-}PP)_{30}$ UTF before and after 20000s OER test.

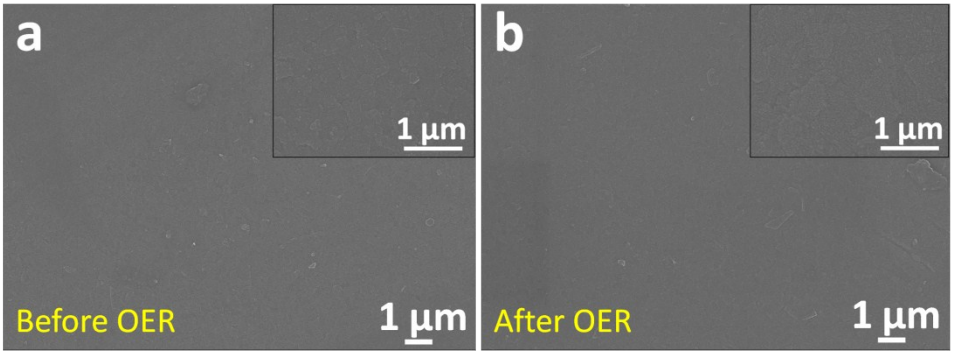

Fig. S19 SEM images of $(CoNi\text{-}LDH/Fe\text{-}PP)_{30}$ UTF (a) before and (b) after 20000s OER test (inset: the enlarged images of $(CoNi\text{-}LDH/Fe\text{-}PP)_{30}$ UTFs).

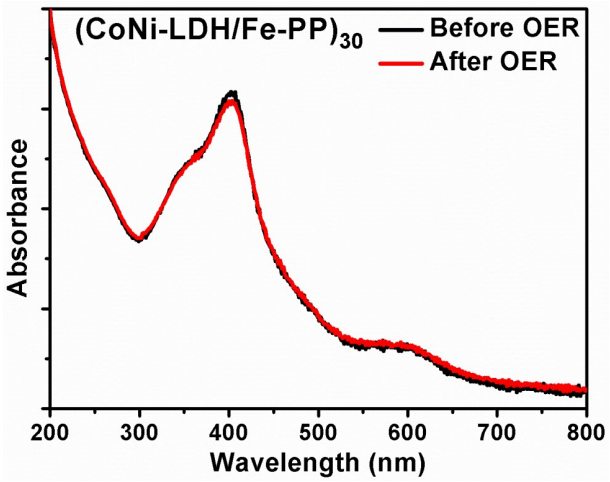

Fig. S20 UV–vis absorption spectra of the $(CoNi\text{-}LDH/Fe\text{-}PP)_{30}$ UTF before and after 20000 s OER.

Fig. S21 Photographs of Pt wire cathode and ITO glass anode of the water-splitting cell driven by a 1.5 V AA battery.

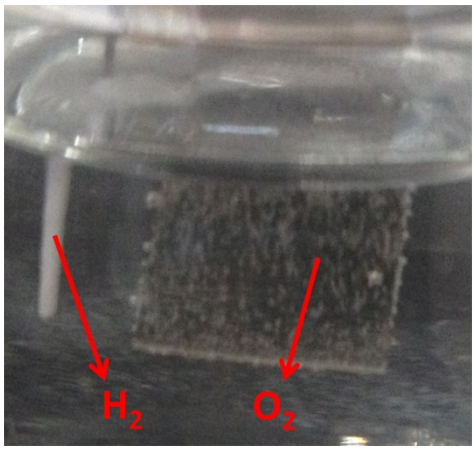

Fig. S22 Cathode and anode of the water-splitting cell when increasing the potential to 1.7 V (*vs*. RHE).

References

1 J. Liang, R. Ma, N. Iyi, Y. Ebina, K. Takada and T. Sasaki, *Chem. Mater.*, 2010, **22**, 371.

2 F. Song and X. Hu, *J. Am. Chem. Soc.*, 2014, **136**, 1648.

3 M. Shao, X. Xu, J. Han, J. Zhao, W. Shi, X. Kong, M. Wei, D. G. Evans and X. Duan, *Langmuir*, 2011, **27**, 8233.

4 X. Zou, A. Goswami and T. Asefa, *J. Am. Chem. Soc.*, 2013, **135**, 17242.

5 Y. Liang, Y. Li, H. Wang, J. Zhou, J. Wang, T. Regier and H. Dai, *Nat. Mater.*, 2011, **10**, 780.

6 F. Song and X. Hu, *Nat. Commun.*, 2014, **5**, 4477.

7 L. Zhou, X. Huang, H. Chen, P. Jin, G. Li and X. Zou, *Dalton Trans.*, 2015, **44**, 11592.

8 Z. Lu, W. Xu, W. Zhu, Q. Yang, X. Lei, J. Liu, Y. Li, X. Sun and X. Duan, *Chem. Commun.*, 2014, **50**, 6479.

9 X. Long, J. Li, S. Xiao, K. Yan, Z. Wang, H. Chen and S. Yang, *Angew. Chem. Int. Ed.*, 2014, **53**, 7584.

10 H. Wang, C. Tang and Q. Zhang, *J. Mater. Chem. A*, 2015, **3**, 16183.

11 C. Tang, H. Wang, H. Wang, Q. Zhang, G. Tian, J. Nie and F. Wei, *Adv. Mater.*, 2015, **27**, 4516.

12 D. H. Youn, Y. B. Park, J. Y. Kim and G. Magesh, *J. Power Sources*, 2015, **294**, 437.

13 W. Ma, R. Ma, C. Wang, J. Liang, X. Liu, K. Zhou and T. Sasaki, *ACS Nano*, 2015, **9**, 1977.

14 X. Yu, M. Zhang, W. Yuan and G. Shi, *J. Mater. Chem. A*, 2015, **3**, 6921.

15 N. Han, F. Zhao and Y. Li, *J. Mater. Chem. A*, 2015, **3**, 16348.

16 M. Gong, Y. Li, H. Wang, Y. Liang, J. Z. Wu, J. Zhou, J. Wang, T. Regier, F. Wei and H. Dai, *J. Am. Chem. Soc.*, 2013, **135**, 8452.

17 D. Tang, Y. Han, W. Ji, S. Qiao, X. Zhou, R. Liu, X. Han, H. Huang, Y. Liu and Z. Kang, *Dalton Trans.*, 2014, **43**, 15119.

18 G. Abellan, J. A. Carrasco, E. Coronado, J. Romeroa and M. Varela, *J. Mater. Chem. C*, 2014, **2**, 3723

19 X. Long, S. Xiao, Z. Wang, X. Zheng and S. Yang, *Chem. Commun.*, 2015, **51**, 1120.

20 C. Qiao, Y. Zhang, Y. Zhu, C. Cao, Xinhua Bao and J. Xu, *J. Mater. Chem. A*, 2015, **3**, 6878.

21 Ying Li, Lu Zhang, Xu Xiang, Dongpeng Yan and Feng Li, *J. Mater. Chem. A*, 2014, **2**, 13250.

22 J. Jiang, A. Zhang, L. Li and L. Ai, *J. Power Sources*, 2015, **278**, 445.

23 H. Liang, F. Meng, M. Caban-Acevedo, L. Li, A. Forticaux, L. Xiu, Z. Wang and Song Jin, *Nano Lett.,* 2015, **15**, 1421.